Bioorganic & Medicinal Chemistry 19 (2011) 5231–5237

Contents lists available at ScienceDirect

Bioorganic & Medicinal Chemistry

journal homepage: www.elsevier.com/locate/bmc

CH/π hydrogen bonds play a role in ligand recognition and equilibrium between active and inactive states of the β2 adrenergic receptor: An ab initio fragment molecular orbital (FMO) study

Tomonaga Ozawa [a,*], Kosuke Okazaki [a], Kazuo Kitaura [b]

[a] Kissei Pharmaceutical Company Ltd, Central Research Laboratory, 4365-1 Kashiwabara, Hotaka, Azumino-City, Nagano-Pref. 399-8304, Japan
[b] Department of Theoretical Drug Design, Graduate School of Pharmaceutical Sciences, Kyoto University, Sakyo-ku, Kyoto 606-8501, Japan

ARTICLE INFO

Article history:
Received 17 May 2011
Revised 1 July 2011
Accepted 2 July 2011
Available online 20 July 2011

Keywords:
CH/π hydrogen bond
Weak hydrogen bond
Weak molecular interaction
An ab initio fragment molecular orbital (FMO) method
G protein-coupled receptors (GPCRs)
β_2 adrenergic receptor
Equilibrium between active and inactive states

ABSTRACT

We examined CH/π hydrogen bonds using an ab initio fragment molecular orbital (FMO) method, combined with the CHPI program, to evaluate complexes of active (bound with agonist **1**) and inactive (bound with inverse agonist **2**) β2 adrenergic receptor (β_2AR) states. In both states, we found that CH/π hydrogen bonds were present. Subtle changes in the binding pocket between the active and inactive states of β_2AR were observed. Comparison of the CH/π networks in both states suggests that the networks differ at the β_2AR core. Recombination of the CH/π hydrogen bonds occurred during conversion between the two states. We suggest that CH/π hydrogen bonds play a key role in ligand recognition and conversion between the active and inactive states.

1. Introduction

G protein-coupled receptors (GPCRs) are involved in many physiological processes, including detection of various extracellular signals and their transduction to the cell interior.[1] More than 800 different GPCRs are present in the human genome.[2,3] GPCRs are activated by a diverse range of endogenous ligands, including biogenic amines, peptides, protein hormones, nucleosides, lipids, and eicosanoids. Indeed, approximately half of all commercially available drugs act on GPCRs. Ligands of GPCRs are classified into four groups, according to their effects: (1) an agonist, which maximally activates the receptor; (2) a partial agonist, which induces sub-maximal activity; (3) a neutral antagonist, which has no effect on basal activity but blocks activity of other ligands; and (4) an inverse agonist that inhibits the basal activity.

X-ray crystal structures of GPCR complexes were determined for bovine rhodopsin in 2000.[4] Structures of β_2-adrenergic GPCR (β_2AR),[5,6] β_1-adrenergic GPCR (β_1AR),[7] and the A_{2A} adenosine receptor (A_{2A})[8] have also been solved. More recently, structures of the dopaminergic receptor 3 (D3)[9] and the CXR4 receptor[10] were solved. These structures have provided evidence that not only hydrogen bonds, but also nonpolar interactions, contribute to ligand recognition by GPCRs.

Involvement of nonpolar interactions during ligand recognition occurs in many GPCRs. For example, Klabunde et al. studied thirteen GCPRs and argued that nonpolar interactions were key elements for GPCR ligand recognition.[11] McAllister et al. noted that CH/π hydrogen bonds are important during ligand binding by the cannabinoid CB1 receptor.[12] For the serotonin 5-HT_6 receptor, Fuente et al. suggested that CH/π hydrogen bonds increased inactive state stability.[13]

In 2011, the structures of β_2AR[14,15], β_1AR[16], and A_{2A}[17], in complex with their agonists, were determined. Comparison of the active and inactive β_2AR structures revealed that the active state binding pocket was subtly different.[15] This change was coupled with an outward movement of the cytoplasmic end of transmembrane 6 (TM6) by 11 Å, triggering binding of the G protein. This movement is closely linked to the packing rearrangement interaction among nonpolar residues, especially Ile121$^{3.40}$ and Phe282$^{6.44}$. These findings suggest that nonpolar interactions are involved in the conversion between the active and inactive states of β_2AR.

Based on these results, we hypothesized that the nonpolar interactions observed in the ligand/GPCR interactions can be attributed

* Corresponding author. Tel.: +81 263828820; fax: +81 263828827.
E-mail address: tomonaga_ozawa@pharm.kissei.co.jp (T. Ozawa).

0968-0896/$ - see front matter © 2011 Elsevier Ltd. All rights reserved.
doi:10.1016/j.bmc.2011.07.004

primarily to CH/π hydrogen bonds. To evaluate this, we used a fragment molecular orbital (FMO) method and program-search using CHPI.[18] The CHPI program was originally used to search short contacts between CH groups and π systems in proteins.[19] This software is now freely available as BioStation Viewer.[20]

The CH/π hydrogen bond is an attractive molecular force, similar to NH/π,[21] OH/π,[22] and CH/O[23] hydrogen bonds. The energy of a single CH/π bond is ca. 1.5–2.5 kcal/mol in, for example, aliphatic and aromatic compounds.[24–26] Analysis of the Cambridge Structural Database (CSD) demonstrated that the distance between a hydrogen atom and the nearest neighboring carbon atom of an aromatic group is approximately 2.9 Å,[27] which corresponds to the sum of the carbon and hydrogen atoms' van der Waals radii. CH/π hydrogen bonds are often observed in biomolecules, and are important in protein-ligand interactions.[28–31] For example, Imamoto et al. found that a single CH/π hydrogen bond governs the stability and bioactivity of photoactive yellow protein.[32] Plevin et al. found that the methyl groups in leucine are involved in the CH/π hydrogen bond by examining NMR coupling constants.[33]

The molecular orbital (MO) method is useful for studying molecular interactions. Sakaki et al. first calculated the energy of the CH/π hydrogen bond at the second-order Møller–Plesset perturbation theory (MP2) level, and concluded that the CH/π hydrogen bond was predominantly stabilized through dispersion interactions.[34] This study was followed by many high-level MO calculations.[35–37]

Applying the MO method to large molecules, such as proteins and nucleic acids, is very challenging. To approach this problem, Kitaura et al. developed a technique known as the fragment molecular orbital (FMO) method.[38–40] Using the FMO method, a protein is divided into fragments (amino acid residues), and MO calculations are performed on each fragment (monomer) and fragment pairs (dimer). The properties of the protein are then estimated based on the individual properties of the monomers and dimers. Furthermore, the inter-fragment interaction energies (IFIEs), obtained using the FMO scheme, correspond to the interaction energies between a ligand and each amino acid residue, when considering a complex between a protein and a ligand. Thus, IFIEs can be used to evaluate various interactions, including the CH/π hydrogen bonds in biomolecules.[41–45]

In this Paper, we examine whether the CH/π hydrogen bonds are involved in GPCR recognition of agonists and inverse agonists. Several CH/π hydrogen bonds have, in fact, been detected using CHPI analysis, and semi-quantified using the FMO method. Further, we demonstrate that changes in the CH/π network reflect differences in the β_2AR active/inactive state structures.

2. Methods

2.1. Molecular modeling

2.1.1. Complex between agonist (1) and β_2AR

The crystal structure was provided pre-complexed with a camelid antibody fragment termed a 'nanobody' (PDB code 3P0G). Because interactions between the nanobody and β_2AR are minimal, the final structure did not include the nanobody region from 3P0G.

2.1.2. Complex between inverse agonist (2) and β_2AR

This crystal structure was provided as a human β_2AR-T4 lysozyme fusion protein (PDB code 2RH1). Because interactions between T4 lysozyme and β_2AR are minimal, the final structure of β_2AR region did not include the T4 lysozyme unit from 2rh1.

2.1.3. Crystal structure refinement

Crystallographic resolutions of the protein/ligand complexes were 3.5, and 2.4 Å for β_2AR/**1** (3P0G) and β_2AR/**2** (2RH1), respectively. Hydrogen atoms were generated using molecular graphic software Discovery Studio 2.5.5 (Accelrys, Inc., San Diego, CA). We assumed that the N-termini of the lysine and arginine side chains were protonated, while the C-termini of aspartic and glutamic side chains were deprotonated. The CHARMm force field implemented in Discovery Studio 2.5.5 was used for the minimization steps. Protein structures were optimized by the steepest descent (SD) method at a dielectric constant of $\varepsilon = 4R$ (R: distance). Optimization was performed stepwise. Initially, structures were minimized under conditions that constrained nonhydrogen atoms. Next, the protein backbone atoms were constrained. At the final step, all atoms were minimized with the harmonic atom constraint. The force constants of the harmonic atom constraints gradually decreased from 100.0 to 10.0, and then to 1.0 kcal/mol Å^2. The positions of heavy atoms in complexes were virtually identical to the original coordinates after minimization; root mean square deviation (RMSD) values of heavy atoms were 0.53 and 0.32 Å for b2AR/1 (3P0G) and b2AR/2 (2RH1), respectively.

2.2. CHPI analysis

CH/π hydrogen bonds were evaluated using the program 'CHPI', implemented in BioStation Viewer.[20] This program determines the distances and angles between CHs and interacting aromatic rings. The criteria for the CH/π hydrogen bonds differ according to the position of the CH hydrogen; a detailed description of the CHPI analysis has been provided previously.[18]

2.3. FMO calculations

Using the FMO method, a molecule or molecular cluster is divided into M fragments (monomers), as shown in Figure 1a. Ab initio calculations are then performed repeatedly on these monomer fragments in the presence of the electrostatic potential created by surrounding (M-1) monomers (V_I), until all the monomer densities become consistent. Next, the dimer equations are solved in the presence of the electrostatic potential from neighboring (M-2) monomers (V^{IJ}). Finally, total energy of the system, E, is written as Eq. 1, using the total energies of the monomer E_I and the dimer E_{IJ}.

$$E = \sum_{I>J}^{M} E_{IJ} - (M-2)\sum_{I}^{M} E_I \tag{1}$$

The internal fragments interaction energy (IFIE) in the FMO calculations are defined by Eq. 2,

$$\Delta E_{IJ} = (E'_{IJ} - E'_I - E'_J) + Tr(\Delta P^{IJ} V^{IJ}) \tag{2}$$

where P^{IJ} is a differential density matrix, V^{IJ} is the environmental electrostatic potential for dimer IJ, and E'_I and E'_{IJ} are the energies of the monomer and the dimer, respectively, in the absence of environmental electrostatic potential.

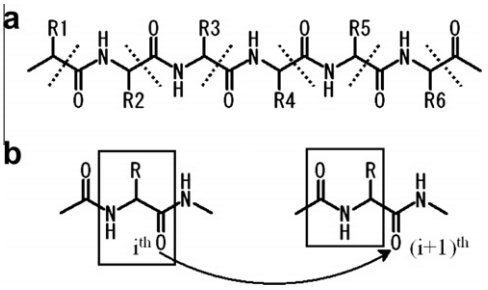

Figure 1. Fragmentation of molecules. (a) The protein was divided into individual amino acid residues. (b) Each carbonyl group (ith) was allocated to the next (i + 1)th residue.

In this study, the protein was divided into single amino acid residues to investigate intermolecular interactions between the protein and ligand, based on the amino acid residues. The fragmented residues did not correspond exactly to each amino acid residue because partitioning of the chemical structure in the FMO scheme was performed between the Cα atom and the main-chain carbonyl group. Thus, the main-chain carbonyl group of the *i*th residue was assigned to the (*i* + 1)th residue fragment (Fig. 1b).

Single-point energy calculations were performed by Hartree–Fock (HF) and second-order Møller–Plesset perturbation (MP2) methods, using the 6-31G basis set (FMO-HF/6-31G and FMO-MP2/6-31G): 4,700 atoms and 25,744 basis functions for complexes between β_2AR and **1**. All FMO calculations were performed with the ABINIT-MP program.[20] Calculations were carried out on a Pentium 4 3.4-GHz cluster (20 CPUs). This system (FMO-MP2/6-31G) required approximately 50 h to analyze the β_2AR and **1** complex.

2.4. Basis set size, BSSE, and overestimation of dispersion energy by the MP2 method

While calculating CH/π hydrogen bonds, the size of the basis set, the basis set superposition error (BSSE), and overestimates of the dispersion energy by the MP2 method must be accounted for. Ishikawa et al.[46] applied a local MP2 method to the FMO scheme, and investigated the basis set dependence on a component of the dispersion energies, namely the individual pair correlation energy ratios of selected orbital pairs to the total dispersion interaction. Using a model compound (CH3OH-C6H6), they showed that the components of the dispersion energies were independent of the basis set size. Ratios of the sum of dispersion energy components in three σ_{CH}/π_{CC} pairs to the total dispersion interaction energies, were 31.2%, 29.4%, 30.8%, 33.1%, 36.3%, and 36.3% using the 6-31G, 6-31G*, 6-31G**, cc-pVDZ, cc-pVTZ, and cc-pVQZ basis sets, respectively. This demonstrates that information regarding the relative importance of dispersion energies can be obtained, even when using small basis sets, such as 6-31G.

Treatment of BSSE in the FMO scheme has not been established. Ishikawa et al.[47] introduced the counterpoise method into the FMO scheme, and showed that interaction energies obtained from FMO calculations can be used in qualitative discussions without correcting for BSSE.

Several high-level ab initio calculations were performed, evaluating CH/π hydrogen bonds. According to Tsuzuki et al.[48] the interaction energies of the benzene-methane complexes obtained using the MP2 method were overestimated by 30%, compared with determined using the CCSD(T) method (cc-pVTZ basis set).

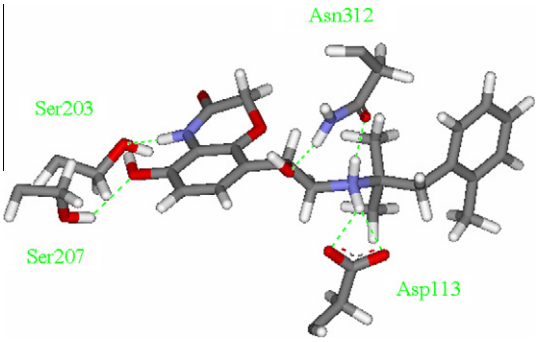

Figure 2. Hydrogen bonds observed between β2AR and **1**. Green dotted lines indicate hydrogen bonds.

Taken together, the FMO/MP2/6-31G results for the CH/π hydrogen bonds are semi-quantitative. The purpose of this study was to examine the role of CH/π hydrogen bonding in the β_2AR. Thus, our semi-quantitative results are useful for studying β_2AR/ligands and intra-residue interactions for drug design.

3. Result and discussion

3.1. β_2AR/agonist complex

CHPI analyses and FMO calculations revealed that agonist **1** (BI-1677107) binds β_2AR through a variety of molecular interactions, including salt bridges, conventional hydrogen bonds, CH/O, and CH/π hydrogen bonds. The interaction energies between 1 and β2AR are summarized in Table 1. As shown in Figure 2, a salt bridge is formed between Asp113$^{3.32}$ (the superscript value refers to Ballesteros numbering for identified amino acid positions for GPCRs: the former figure is the transmembrane number and the latter is the position of the residue) and the ethanolamine component of 1 (interaction energy of −107.3 kcal/mol). This Asp is highly conserved in biogenic-amine binding GPCRs. Two hydrogen bonds are formed between Asn312$^{7.39}$ and the ethanolamine domain of **1** (interaction energy of −30.5 kcal/mol). These three interactions are common among agonists and inverse agonists of β_2AR.

The desolvation energy relates to the competition between the protein–ligand interaction and their interactions with water.[49] This is an important contribution to the binding of ligand to protein, and is more important in membrane proteins, such as GPCRs, because the ligand must be completely desolvated to bind to the receptor.[50] This desolvation penalty is essential for a polar or charged system,

Table 1
Interaction energies (in kcal/mol) between β2AR and ligands **1** and **2**

	Agonist (BI-167107 **1**)			Inverse agonist (Carazolol **2**)			Changes
	E_{MP2}[a]	E_{RHF}[b]	$\Delta E_{MP2\text{-}RHF}$[c]	E_{MP2}[a]	E_{RHF}[b]	$\Delta E_{MP2\text{-}RHF}$[c]	ΔE_{MP2}[d]
Asp113$^{3.32}$	−107.3	−100.2	−7.1	−134.8	−126.9	−7.9	27.5
Asn312$^{7.39}$	−30.5	−24.9	−5.6	−29.3	−24.2	−5.1	−1.2
Ser203$^{5.42}$	−10.2	−7.1	−3.1	−4.6	−2.7	−1.9	−5.6
Tyr308$^{7.35}$	−8.2	−5.3	−3.0	−6.1	−4.9	−1.2	−2.1
Phe193$^{5.32}$	−7.9	3.0	−10.9	−3.3	1.0	−4.3	−4.6
Ser204$^{5.43}$	−5.0	−3.4	−1.5	−5.4	−2.8	−2.6	0.4
Phe290$^{6.52}$	−4.8	−1.7	−3.1	−3.8	0.7	−4.5	−1.0
Phe289$^{6.51}$	−4.7	−0.6	−4.1	−4.6	0.1	−4.7	−0.1
Trp286$^{6.48}$	−3.4	−2.8	−0.6	−5.3	−2.7	−2.7	2.0
Val114$^{3.33}$	−3.1	1.5	−4.6	−4.8	0.4	−5.2	1.7
Ser207$^{5.46}$	−2.8	−1.1	−1.7	2.1	3.1	−1.1	−4.9

[a] Interaction energies calculated at the MP2/6-31G level.
[b] Interaction energies calculated at the RHH/6-31G level.
[c] $E_{MP2} - E_{RHF}$ in kcal/mol.
[d] Changes in the interaction energies between agonist **1** (active) and inverse agonist **2** (inactive); $\Delta E_{MP2} = E_{MP2}$(Agonist **1**) − E_{MP2}(Inverse agonist **2**) at the MP2/6-31G level.

Table 2
CH/π distances between β_2AR and ligands **1** and **2**

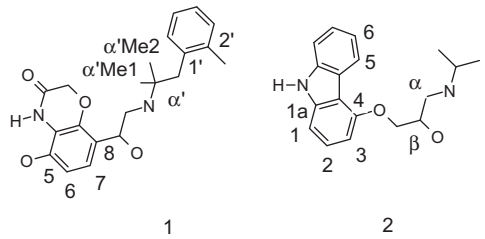

Agonist (BI-1671071 **1**)					Inverse agonist (Carazolol **2**)				
π acceptor		π donor		Distance[a]	π acceptor		π donor		Distance[a]
Ligand	6	Val114	CHγ	2.9	Ligand	3	Val114	CHα	3.0
Ligand	7	Val114	CHγ	3.0	Ligand	2	Val114	CHγ	2.7
Ligand	8	Phe289	CHε2	3.0	Ligand	4	Val114	CHγ	3.0
Ligand	6	Phe290	CHζ	2.9	Ligand	1a	Phe290	CHε2	2.8
Ligand	2'	Phe193	CHβ	2.9	Ligand	3	Phe290	CHζ	2.7
Phe193	Cγ	Ligand	α'MeH1	2.9	Ligand	6	Phe193	CHε2	2.9
Phe193	Cδ	Ligand	α'MeH2	2.9	Phe289	Cζ	Ligand	CHβ	2.8

[a] H/C inter atomic distance in Å.

because the interaction between ligand and water is primarily an electrostatic interaction. Interaction energies between Asp113$^{3.32}$ and Asn312$^{7.39}$ and **1** would be markedly reduced by the desolvation penalty. In contrast, desolvation has little effect on the dispersion interaction. As a result, other interactions, mentioned below, also contribute to the binding of 1 to β2AR.

Three serine residues in TM5 (Ser203$^{5.42}$, Ser204$^{5.43}$, and Ser207$^{5.46}$) are important for the binding of agonists. The heterocyclic component of **1** interacts with Ser203$^{5.42}$ and Ser207$^{5.46}$ through hydrogen bonds (interaction energies of −10.2 and −2.8 kcal/mol, respectively). The interaction energy of Ser204$^{5.43}$ (−5.0 kcal/mol) is attributed to the CH/O hydrogen bond between the hydroxyl group of **1** and the carbonyl oxygen of Ser203$^{5.42}$, which is allocated to Ser204$^{5.43}$ due to the FMO fragmentation rule (Fig. 1). This indicates that Ser204$^{5.43}$ does not interact directly with **1**.

Using CHPI analysis, four residues (Val114$^{3.33}$, Phe193$^{5.32}$, Phe289$^{6.51}$, and Phe290$^{6.52}$) were been found to have short CH/π contacts with **1** (Table 2). As shown in Figure 3a, the heterocyclic ring

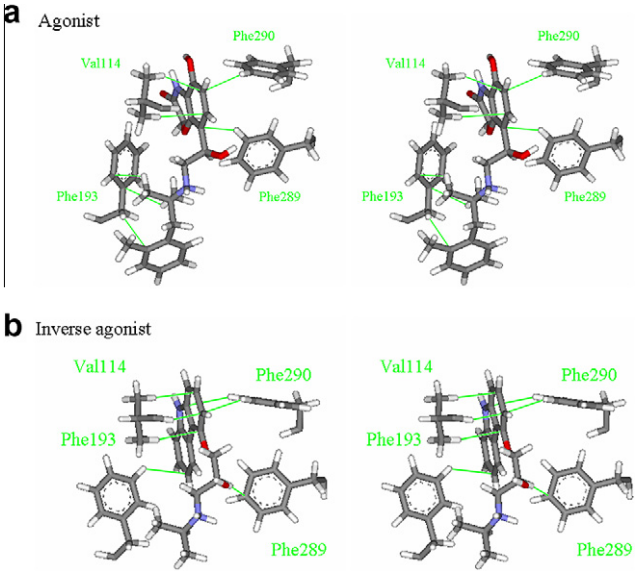

Figure 3. CH/π hydrogen bonds observed between β_2AR and ligands **1** and **2** (stereo view). Green lines indicate CH/π hydrogen bonds.

of **1** is located between Phe289, Phe290, and Val114. The interaction energies are estimated to be −4.7, −4.8, and −3.1 kcal/mol for Phe289$^{6.51}$, Phe290$^{6.52}$, and Val114$^{3.33}$, respectively. The interaction energies are significantly larger than those obtained from HF calculations: −4.7 versus −0.6, −4.8 versus −1.7, and −3.1 versus 1.5 kcal/mol for Phe289$^{6.51}$, Phe290$^{6.52}$, and Val114$^{3.33}$, respectively. This suggests that dispersion energies are primarily responsible for interactions between the three residues and **1**. The interaction energy between Phe193$^{5.32}$ and **1** is −7.9 kcal/mol, corresponding to three CH/π and one NH/π short contact. Phe193$^{5.32}$ functions as a CH acceptor (π donor), as well as a CH donor.

The CH/O hydrogen bond was found in Tyr308$^{7.35}$. The interaction energy is −8.2 kcal/mol, and the distance between the hydrogen of **1** and the phenoxy oxygen of Tyr308$^{7.35}$ is 2.6 Å. Neither hydrogen bonds nor CH/π hydrogen bonds were observed between **1** and Tyr308. Thus, this interaction can be attributed to the CH/O hydrogen bond.

In summary, agonist **1** (BI-167107) is recognized through a variety of molecular interactions, including salt bridges, conventional hydrogen bonds, CH/O, NH/π, and CH/π hydrogen bonds. Figure 4 summarized these interactions between β_2AR and **1**.

3.2. β_2AR/inverse agonist complex

Inverse agonist **2** (carazolol) binds to β_2AR through a variety of molecular interactions, including salt bridges, conventional

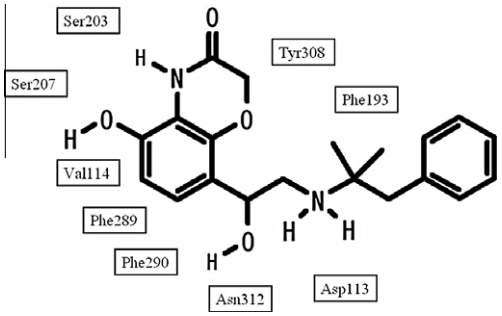

Figure 4. Interaction map between β_2AR and **1**: Asp113, salt bridge hydrogen bond; Ser203, Ser207, and Asn312, conventional hydrogen bonds; Phe193, NH/π hydrogen bond; Tyr308, CH/O hydrogen bond; Val114, Phe193, Phe289, and Phe290, CH/π hydrogen bonds.

hydrogen bonds, CH/O, and CH/π hydrogen bonds, similar to the agonist **1**/β_2AR complex. The interaction energies between **2** and β_2AR are summarized in Table 1. A salt bridge is formed between Asp113$^{3.32}$ and the amine component of **2** (interaction energy of −134.8 kcal/mol). Two hydrogen bonds are formed between Asn312$^{7.39}$ and the ethanolamine component of **2** (interaction energy of −29.3 kcal/mol). Interaction energies between Asp113$^{3.32}$ and Asn312$^{7.39}$ and **2** would be markedly reduced by the desolvation penalty, as well as the interaction of **1**.

The carbazole component of **2** interacts with Ser203$^{5.42}$ through hydrogen bonds (interaction energies of −4.6 kcal/mol). Ser207$^{5.46}$ has unattractive energies (+2.1 kcal/mol), while agonist **1** has attractive energies (−2.8 kcal/mol). Interactions with these serines differ between the agonist and inverse agonist.

Based on CHPI analysis, four residues (Val114$^{3.33}$, Phe193$^{5.32}$, Phe289$^{6.51}$, and Phe290$^{6.52}$) were been found to have short CH/π contacts with **2** (Table 2, Fig. 3b). The interactions with Val114$^{3.33}$ and Phe290$^{6.52}$ are similar to that of β_2AR/**1**, but the interaction modes of Phe193$^{5.32}$ and Phe289$^{6.51}$ are different between the two ligands. The carbazole ring of **2** is surrounded by Val114$^{3.33}$, Phe193$^{5.32}$, and Phe290$^{6.52}$. Phe193$^{5.32}$ interacts with the aromatic component of **2**, instead of Phe289$^{6.51}$, as seen in the β_2AR/**1** complex. The interaction energies are estimated to be −4.8, −3.3, and −3.8 kcal/mol for Val114$^{3.33}$, Phe193$^{5.32}$, and Phe290$^{6.52}$, respectively. Phe289 is oriented towards the β hydrogen of **2**, while in β_2AR/**1**, Phe289 acts as a CH donor. Versatility in the CH/π hydrogen bonds may allow for binding to both ligands.

The CH/O hydrogen bond was found in Trp286$^{6.48}$. The interaction energy is −5.3 kcal/mol, and the distance between the alcohol oxygen of **2** and the η hydrogen of Trp286$^{6.48}$ is 2.6 Å. No hydrogen bond or CH/π hydrogen bond is observed between **2** and Trp286$^{6.48}$. Thus, this interaction is attributed to the CH/O hydrogen bond.

In summary, inverse agonist **2** (carazolol) is recognized through a variety of molecular interactions, including salt bridges, conventional hydrogen bonds, CH/O, and CH/π hydrogen bonds. Interactions of **2** with β_2AR are similar to **1**/β_2AR, but there are some important differences. These differences are discussed in the following section.

3.3. Comparison of ligand interactions in the active and inactive states

According to Kobilka et al. a conformational change in Ser203$^{5.42}$ and Ser207$^{5.46}$ occurs when agonist **1** is bound to β_2AR, allowing for larger conformational changes in the cytoplasmic region. This is associated with an alteration in the ligand/β_2AR interaction. Table 1 lists the interaction energies changes when β_2AR is bound to agonist **1** (active state) and inverse agonist **2** (inactive state). This is described mathematically as $\Delta E_{MP2} = E_{MP2}$(agonist **1**) − E_{MP2}(inverse agonist **2**). Interactions in the active state (**1**/β_2AR) for Ser203$^{5.42}$ and Ser207$^{5.46}$ are markedly stabilized, compared with the inactive state (**2**/β_2AR). The energies are −5.6 and −4.9 kcal/mol, respectively, for Ser203$^{5.42}$ and Ser207$^{5.46}$.

The interaction modes of Asp113$^{3.32}$ (salt bridge) and Asn312$^{7.39}$ (hydrogen bond) are similar in the two states. However, the interaction energies of Asp113$^{3.32}$ are distinct from each other: −134.8 (inactive state) and −107.3 kcal/mol (active state). This may be related to ligand affinity.

No change is observed in the conformation of Trp286$^{6.48}$ between the active and inactive states, although the side chain of this tryptophan is believed to rotate when the GPCR is activated. The interaction energies of the β_2AR are −3.4 and −5.3 kcal/mol for the agonist and inverse agonist, respectively. The proximal distances of Trp286$^{6.48}$ and ligands (the alcohol oxygen of the ligands and the indole hydrogen of Trp286$^{6.48}$) are 3.8 and 2.6 Å, respectively. Involvement of the CH/O hydrogen bond, discussed in the previous section, may explain the role of Trp286$^{6.48}$ in shifting between the two states.

Val114$^{3.33}$, Phe289$^{6.51}$, and Phe290$^{6.52}$ interact with β_2AR through CH/π hydrogen bonds in both states. These three residues are highly conserved among adrenergic receptors (β_{1-3}, α_{1A}, α_{1B}, α_{1D}, α_{2A}, α_{2B}, and α_{2C}), dopaminergic receptors (D_{1-5}), and serotonergic receptors (5-HT$_{1A}$, 5-HT$_{1B}$, 5-HT$_{1D}$, 5-HT$_{1E}$, 5-HT$_{1F}$, 5-HT$_{2A}$, 5-HT$_{2B}$, 5-HT$_{2C}$, 5-HT$_4$, 5-HT$_{5A}$, 5-HT$_6$, and 5-HT$_7$).[51] These GPCR ligands are almost exclusively composed of aromatic rings and amine components. Thus, the CH/π hydrogen bonds contribute to ligand recognition by the above GPCRs.

FMO results provide interaction energies between ligand and GPCRs, allowing for semi-quantitative analysis. Thus, the FMO method is useful for analyzing GPCR states.

3.4. Conversion of the CH/π network is dependent on the receptor state

Kobilka et al. proposed that conversion between the active and inactive states of β_2AR are associated with changes in hydrophobic packing. We hypothesized that CH/π hydrogen bonds contribute significantly to the receptor state shift. CH/π hydrogen bonds effects on β_2AR states were examined with regard to the CH/π network.

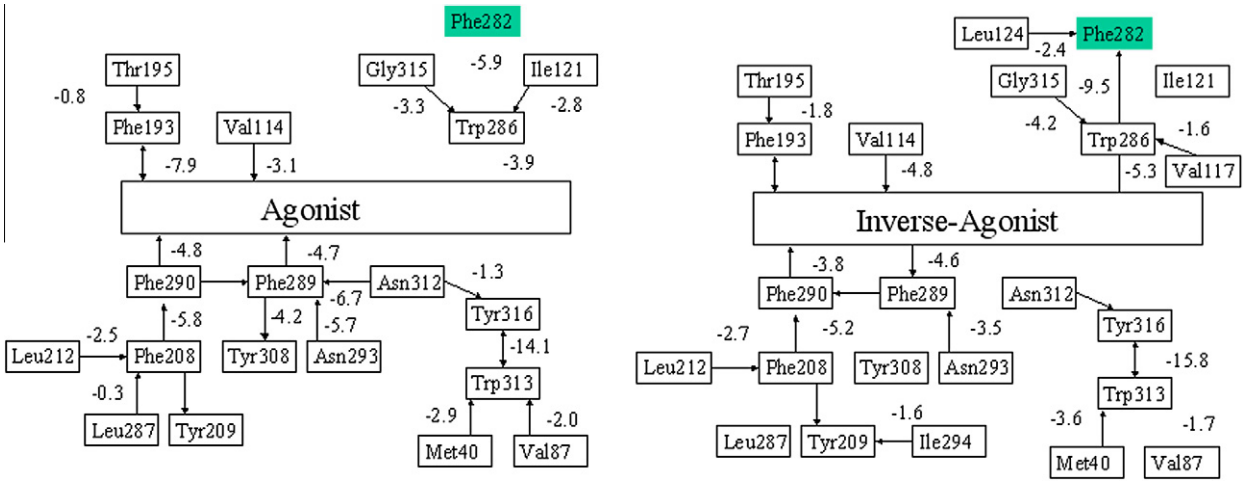

Figure 5. Comparison of the CH/π networks observed in active and inactive states, indicating that CH/π hydrogen bond and interaction energies between two residues.

Two states were analyzed by CHPI and FMO calculations. CHPI can search for inter-residue CH/π hydrogen bonds occurring in proteins, and FMO calculations can evaluate inter-residue interactions. Combining the two methods allows semi-quantification of the CH/π network. Figure 5 shows the CH/π network and interaction energies among residues surrounding the agonist and inverse agonist. Arrows and lines indicate CH/π hydrogen bonds and hydrogen bonds, respectively, and the direction of the arrows shows the direction of the CH donor to π acceptor interaction. This CH/π network extends broadly from the cell surface to the transmembrane region core. The network is composed of Ile294$^{6.56}$, Tyr209$^{5.48}$, Phe208$^{5.47}$, Phe290$^{6.52}$, Phe289$^{6.51}$, inverse agonist, Trp286$^{6.48}$, Phe282$^{6.44}$, and Leu124$^{3.43}$, in the inactive state. In contrast, the interaction network was cleaved at Trp286$^{6.48}$ and Phe282$^{6.44}$ in the active state. This difference in extension of the CH/π network may contribute to the inactive state stability, compared with the active state.

Agonist binding was accompanied by repositioning of Phe282$^{6.44}$, and loosed of CH/π hydrogen bonds in the active state. Phe282$^{6.44}$ is stabilized by the CH/π hydrogen bonds of Trp286$^{6.48}$ and Leu124$^{3.43}$ in the inactive state, while no CH/π hydrogen bond is observed in the active sates. The conformational shift of Phe282$^{6.44}$ is closely linked to a TM6 rotation, leading to an outward movement of the cytoplasmic end of TM6 (Fig. 6). Loss of the CH/π hydrogen bonds could allow Phe282$^{6.44}$ to shift during activation.

Ile121$^{3.40}$ forms CH/π hydrogen bonds with Trp286$^{6.48}$ only in the active state. Conformational changes in Ile121$^{3.40}$ were observed during activation of β_2AR. It seems likely that this CH/π hydrogen bond prevents the interaction between Phe282 and Trp286, leading to inactivation of β_2AR.

The movement of Ser203$^{5.42}$ and Ser207$^{5.46}$, accompanied by binding of the agonist, leads to the inward movement of TM5, including a 2.1 and 1.4 Å shift at positions Ser207$^{5.46}$ and Pro211$^{5.50}$, relative to the inactive state. The movement of Pro211$^{5.50}$ causes repositioning of Ile121$^{3.40}$, forming a CH/π hydrogen bond with Trp286$^{6.48}$. The formation of this CH/π hydrogen bond interferes with the Phe282$^{6.44}$ and Trp286$^{6.48}$ interaction. As a result, Phe282$^{6.44}$ shifts its position, resulting in an outward movement of TM6, which can then bind the G protein. The recombination of CH/π hydrogen bonds (Trp286/Phe282 in the inactive state, Trp286/Ile121 in the active state) appears to function as a molecular switch (Fig. 7). Mutations of Phe282$^{6.44}$ (F282L, F282A, and F282G) were constitutively active, meaning the receptor has activity in the absence of the ligand.[52] This supports the hypothesis that the CH/π hydrogen bond of Trp286$^{6.48}$/Phe282$^{6.44}$ is stabilized in the inactive state. We discuss interaction changes for Phe282$^{6.44}$ in the following section.

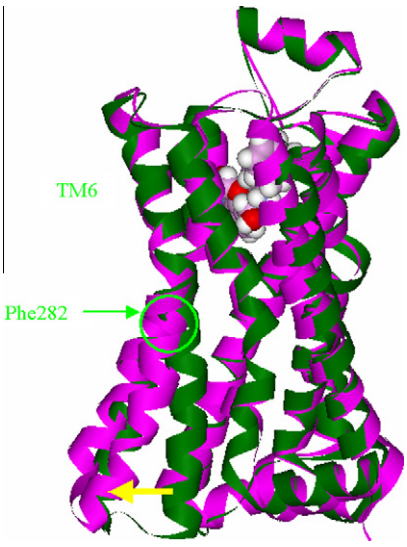

Figure 6. Movement TM6 accompanied with binding of an agonist. Magenta indicates the active state and green indicates the inactive state.

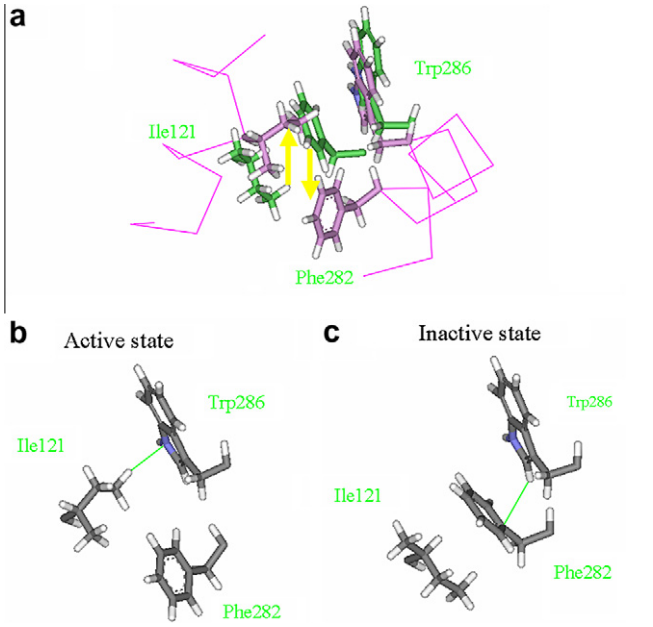

Figure 7. Conformational change of Phe282$^{6.44}$. (a) Superposition of the active and inactive states. Magenta indicates the active state and green indicates the inactive state. Magenta line indicates the back bone of β_2AR. (b) Active state. (c) Inactive state.

Table 3
Comparison of the interaction energies (in kcal/mol) for Phe282$^{6.44}$ in active and inactive states

	Active E_{MP2}[a]	Inactive E_{MP2}[a]	Changes ΔE_{MP2}[b]
Cys285	−0.1	−5.6	5.5
Trp286	−5.9	−9.5	3.6
Thr118	0.0	−3.6	3.6
Asp79	1.5	−0.9	2.4
Glu122	0.3	−1.0	1.3
Leu124	−1.2	−2.4	1.2
Val117	0.1	−1.1	1.2
Asn318	4.0	5.0	−1.0
Ile121	−1.4	−0.4	−1.0
Leu212	−1.5	−0.2	−1.3

[a] Interaction energies calculated at the MP2/6-31G level.
[b] Changes in the interaction energies between active and inactive state; $\Delta E_{MP2} = E_{MP2}$(agonist **1** binding) − E_{MP2}(inverse agonist **2** binding) at the MP2/6-31G level.

3.5. Differences in interaction energies for Phe282$^{6.44}$

The Phe282$^{6.44}$ shift is critical for conversion between β_2AR states. Table 3 lists the interaction energies between Phe282$^{6.44}$ and other residues in the active and inactive states. Residue changes of over 1 kcal/mol between the two states are displayed.

Phe282$^{6.44}$ was destabilized in the active state, compared with the inactive state: Cys285$^{6.47}$ (5.5 kcal/mol), Trp286$^{6.48}$ (3.6 kcal/mol), and Thr118$^{3.37}$ (3.6 kcal/mol). Destabilization of Cys285$^{6.47}$ results from a hydrogen bond break between the carbonyl oxygen of Thr281$^{6.43}$ and the amide nitrogen of Cys285$^{6.47}$. Because of the FMO fragment rule, the main-chain carbonyl group of *i*th residue

was assigned to the $(i+1)$th residue fragment (Fig. 1b). The observed change between Phe282$^{6.44}$ and Trp286$^{6.48}$ is attributed to loss of the CH/π hydrogen bond. Agonist binding shifted the orientation of Phe282$^{6.44}$ from TM3 to TM5, eliminating the interaction with Thr118$^{3.37}$. This interaction is similar to a CH/O hydrogen bond between the carbonyl oxygen of Val117$^{3.36}$ and the phenyl hydrogen in Phe282$^{6.44}$. Phe282$^{6.44}$ was destabilized through loss of the conventional hydrogen bonds, and weak hydrogen bonds (CH/π and CH/O), in the active state, causing Phe282$^{6.44}$ to shift.

4. Conclusions

Interaction energies were calculated using the ab initio FMO method for β_2AR in the active (agonist binding) and inactive (inverse agonist) states. Many nonpolar interactions, including CH/π hydrogen bonds, were found in both states. Using CHPI analysis, it has been found that the CH/π network broadly extends from the cell surface to the core transmembrane region, and is involved in a dynamic equilibrium between the active and inactive states. In particular, Phe282$^{6.44}$, which shifts its position during activation, is destabilized by loss of both the conventional hydrogen bonds and CH/π and CH/O hydrogen bonds. Recombination of the CH/π hydrogen bonds occurred during conversion of the receptor state. The CH/π hydrogen bond appears to function as a switch for β_2AR.

Acknowledgments

We thank Dr. Motohiro Nishio (The CHPI Institute) for discussion and reading the manuscript, and T.O. acknowledges professional technical support through the 'Research and Development of Innovative Simulation Software' (RISS) project of the Ministry of Education, Culture, Sports, Science, and Technology.

References and notes

1. Klabunde, T.; Hessler, G. *ChemBioChem* **2002**, *3*, 928.
2. Fredriksson, R.; Lagerström, M. C.; Lundin, L.-G.; Schiöth, H. B. *Mol. Pharmacol.* **2003**, *63*, 1256.
3. Vassilatis, D. K.; Hohmann, J. G.; Zeng, H.; Li, F.; Ranchalis, J. E.; Mortrud, M. T.; Brown, A.; Rodriguez, S. S.; Weller, J. R.; Wright, A. C.; Bergmann, J. E.; Gaitanaris, G. A. *Proc. Natl. Acad. Sci. U.S.A.* **2003**, *100*, 4903.
4. Palczewski, K.; Kumasaka, T.; Hori, Tetsuya; Behnke, C. A.; Motoshima, H.; Fox, B. A.; Trong, I. L.; Teller, D. C.; Okada, T.; Stenkamp, R. E.; Yamamoto, M.; Miyano, M. *Science* **2000**, *289*, 739.
5. Rasmussen, S. G.; Choi, H.; Rosenbaum, D. M.; Kobilka, T. S.; Thian, F. S.; Edwards, P. C.; Burghammer, M.; Ratnala, V. R.; Sanishvili, R.; Fischetti, R. F.; Schertler, G. F.; Weis, W.; Kobilka, B. K. *Nature* **2007**, *450*, 383.
6. Cherezov, V.; Rosenbaum, D. M.; Hanson, M. A.; Rasmussen, S. G.; Thian, F. S.; Kobilka, T. S.; Choi, H.; Kuhn, P.; Weis, W. I.; Kobilka, B. K.; Stevens, R. C. *Science* **2007**, *318*, 1258.
7. Warne, T.; Serrano-Vega, M. J.; Baker, J. G.; Moukhametzianov, R.; Edwards, P. C.; Henderson, R.; Leslie, A. G.; Tate, C. G.; Schertle, G. F. *Nature* **2008**, *454*, 486.
8. Jaakola, V.; Griffith, M. T.; Hanson, M. A.; Cherezov, V.; Chien, E. T.; Lane, J. R.; Ijzerman, A. P.; Stevens, R. C. *Science* **2008**, *322*, 1211.
9. Chien, E. Y.; Liu, W.; Zhao, W.; Katritch, V.; Han, G. W.; Hanson, M. A.; Shi, L.; Newman, A. H.; Javitch, J. A.; Cherezov, V.; Stevens, R. C. *Science* **2010**, *330*, 1091.
10. Wu, B.; Chien, E. Y.; Mol, C. D.; Fenalti, G.; Liu, W.; Katritch, V.; Abagyan, R.; Brooun, A.; Wells, P.; Bi, F. C.; Hamel, D. J.; Kuhn, P.; Handel, T. M.; Cherezov, V.; Stevens, R. C. *Science* **2010**, *330*, 1066.
11. Klabunde, T.; Giegerich, C.; Evers, A. *J. Med. Chem.* **2009**, *52*, 2932.
12. McAllister, S. D.; Rizvi, G.; Anavi-Goffer, S.; Hurst, D. P.; Barnett-Norris, J.; Lynch, D. L.; Reggio, P. H.; Abood, M. E. *J. Med. Chem.* **2003**, *46*, 5139.
13. Fuente, T.; Martín-Fontecha, M.; Sallander, J.; Benhamú, B.; Campillo, M.; Medina, R. A.; Pellissier, L. P.; Claeysen, S.; Dumuis, A.; Pardo, L.; López-Rodríguez, M. L. *J. Med. Chem.* **2010**, *53*, 1357.
14. Rasmussen, S. G.; Choi, H.; Fung, J. J.; Pardon, E.; Casarosa, P.; Chae, P. S.; DeVree, B. T.; Rosenbaum, D. M.; Thian, F. S.; Kobilka, T. S.; Schnapp, A.; Konetzki, I.; Sunahara, R. K.; Gellman, S. H.; Pautsch, A.; Steyaert, J.; Weis, W. I.; Kobilka, B. K. *Nature* **2011**, *469*, 175.
15. Rosenbaum, D. M.; Zhang, C.; Lyons, J. A.; Holl, R.; Aragao, D.; Arlow, D. H.; Rasmussen, S. G.; Choi, H.; DeVree, B. T.; Sunahara, R. K.; Chae, P. S.; Gellman, S. H.; Dror, R. O.; Shaw, D. E.; Weis, W. I.; Caffrey, M.; Gmeiner, P.; Kobilka, B. K. *Nature* **2011**, *469*, 236.
16. Warne, T.; Moukhametzianov, R.; Baker, J. G.; Nehmé, R.; Edwards, P. C.; Leslie, A. G.; Schertler, G. F.; Tate, C. G. *Nature* **2011**, *469*, 241.
17. Xu, F.; Wu, H.; Katritch, V.; Han, G. W.; Jacobson, K. A.; Gao, Z. G.; Cherezov, V.; Stevens, R. C. *Science* **2011**, *332*, 322.
18. Umezawa, Y.; Tsuboyama, S.; Honda, K.; Uzawa, J.; Nishio, M. *Bull. Chem. Soc. Jpn.* **1998**, *71*, 1207.
19. Umezawa, Y.; Nishio, M. *Bioorg. Med. Chem.* **1998**, *6*, 493.
20. http://www.ciss.iis.u-tokyo.ac.jp/rss21/theme/life/synergy/synergy_software-info.html.
21. Oki, M.; Mutai, K. *Bull. Chem. Soc. Jpn.* **1966**, *39*, 809.
22. Oki, M.; Iwamura, H. *Bull. Chem. Soc. Jpn.* **1959**, *32*, 1135.
23. Pierce, A. C.; Haar, E.; Binch, H. M.; Kay, D. P.; Patel, S. R.; Li, P. *J. Med. Chem.* **2005**, *48*, 1278.
24. Nishio, M.; Umezawa, Y.; Honda, K.; Tsuboyama, S.; Suezawa, H. *Cryst. Eng. Commun.* **2009**, *11*, 1757.
25. Takahasi, O.; Kohono, Y.; Nishio, M. *Chem. Rev.* **2010**, *110*, 6049.
26. Nishio, M. *Phys. Chem. Chem. Phys.* **2011**, 13, doi:10.1039/C1CP20404A.
27. Takahashi, H.; Umezawa, Y.; Tsuboyama, S.; Uzawa, J.; Nishio, M. *Tetrahedron* **1999**, *55*, 10047; Takahashi, H.; Tsuboyama, S.; Umezawa, Y.; Honda, K.; Nishio, M. *Tetrahedron* **2000**, *56*, 6185; Suezawa, H.; Yoshida, T.; Umezawa, Y.; Tsuboyama, S.; Nishio, M. *Eur. J. Inorg. Chem.* **2002**, 3148.
28. Weiss, M. S.; Brandl, M.; Sühnel, J.; Pal, D.; Hilgenfeld, R. *Trends. Biochem. Sci.* **2001**, *26*, 521.
29. Toth, G.; Bowers, S. G.; Truong, A. P.; Probst, G. *Curr. Pharm. Des.* **2007**, *13*, 3476.
30. Umezawa, Y.; Nishio, M. *Bioorg. Med. Chem.* **2000**, *8*, 2643.
31. Umezawa, Y.; Nishio, M. *Biopolymers* **2005**, *79*, 248.
32. Harigai, M.; Kataoka, M.; Imamoto, Y. *J. Am. Chem. Soc.* **2006**, *128*, 10646.
33. Plevin, M. J.; Bryce, D. L.; Boisbouvier *J. Nat. Chem.* **2010**, *2*, 466.
34. Sakaki, S.; Kato, K.; Miyazaki, T.; Musashi, Y.; Ohkubo, K.; Ihara, H.; Hirayama, C. *J. Chem. Soc. Faraday Trans.* **1993**, *89*, 659.
35. Shibasaki, K.; Fujii, A.; Mikami, N.; Tsuzuki, S. *J. Phys. Chem. A* **2007**, *111*, 753.
36. Ran, J.; Wong, M. W. *J. Phys. Chem. A* **2006**, *110*, 9702.
37. Gil, A.; Branchadell, V.; Bertran, J.; Oliva, A. *J. Phys. Chem. B* **2007**, *111*, 9372.
38. Kitaura, K.; Sawai, T.; Asada, T.; Nakano, T.; Uebayasi, M. *Chem. Phys. Lett.* **1999**, *312*, 319.
39. Nakano, T.; Kaminuma, T.; Sato, T.; Akiyama, Y.; Uebayasi, M.; Kitaura, K. *Chem. Phys. Lett.* **2000**, *318*, 614.
40. Fedorov, D. G.; Kitaura, K. *The Fragment Molecular Orbital Method Practical Application to Large Molecular Systems*; CRC Press: New York, 2009.
41. Fukuzawa, K.; Mochizuki, Y.; Tanaka, S.; Kitaura, K.; Nakano, T. *J. Phys. Chem. B* **2006**, *110*, 16102.
42. Takematsu, K.; Fukuzawa, K.; Omagari, K.; Nakajima, S.; Nakajima, K.; Mochizuki, Y.; Nakano, T.; Watanabe, H.; Tanaka, S. *J. Phys. Chem. B* **2009**, *113*, 4991.
43. Nakanishi, I.; Fedorov, D. G.; Kitaura, K. *Proteins: Struct. Funct. Bioinformatics* **2007**, *68*, 145.
44. Ozawa, T.; Okazaki, K. *J. Comput. Chem.* **2008**, *29*, 2656.
45. Ozawa, T.; Tsuji, E.; Ozawa, M.; Handa, C.; Mukaiyama, H.; Nishimura, T.; Kobayashi, S.; Okazaki, K. *Bioorg. Med. Chem.* **2008**, *16*, 10311.
46. Ishikawa, T.; Mochizuki, Y.; Amari, S.; Nakano, T.; Tanaka, S.; Tanaka, K. *Chem. Phys. Lett.* **2008**, *463*, 189.
47. Ishikawa, T.; Ishikura, T.; Kuwata, K. *J. Comput. Chem.* **2009**, *30*, 2594.
48. Tsuzuki, S.; Honda, K.; Uchimaru, T.; Mikami, M.; Tanabe, K. *J. Am. Chem. Soc.* **2000**, *122*, 3746.
49. Mysinger, M. M.; Shoichet, B. K. *J. Chem. Inf. Model* **2010**, 50, 1561.
50. González, A.; Murcia, M.; Benhamú, B.; Campillo, M.; López-Rodríguez, M. L.; Pardo, L. *Med. Chem. Commun.* **2011**, 2, 160.
51. Gloriam, D. E.; Foord, S. M.; Blaney, F. K.; Garland, S. L. *J. Med. Chem.* **2009**, *52*, 4429.
52. Chen, S.; Lin, F.; Xu, M.; Riek, R. P.; Novotny, J.; Graham, R. M. *Biochemistry* **2002**, *41*, 6045–6053.